Photon number and timing resolution of a near-infrared continuous-wave source with a transition-edge sensor

Jianwei Lee,[1, *] Lijiong Shen,[1, 2] Alessandro Cerè,[1] Thomas Gerrits,[3]
Adriana E. Lita,[3] Sae Woo Nam,[3] and Christian Kurtsiefer[1, 2]

[1] *Center for Quantum Technologies, National University of Singapore, 3 Science Drive 2, Singapore, 117543*
[2] *Department of Physics, National University of Singapore, 2 Science Drive 3, Singapore, 117542*
[3] *National Institute of Standards and Technology (NIST), 325 Broadway, Boulder, Colorado 80305, USA*
(Dated: July 25, 2017)

Transition-edge sensors (TES) are calorimetric spectrometers that have near unit efficiency and are photon-number resolving. A recovery time on the order of microseconds, however, limits the number resolving ability and timing accuracy in high photon-flux conditions. This can be addressed by pulsing the light source or discarding overlapping signals, thereby limiting its applicability. A method that works for stationary light sources uses the differentiated TES signal to determine the detection time of overlapping signals and to count photons [1]. However, the low signal-to-noise ratio of TES response when detecting near-infrared photons complicates the direct estimation of their detection times by this method. Here, we present an alternative approach where we use a discriminator inherently robust against noise to coarsely locate pulses in time, the integral of the identified signal regions to count photons, and a separate fit to determine the exact detection instant.

I. INTRODUCTION

Transition-edge sensors were introduced as calorimetric photodetectors based on superconductors for soft X-rays in the past, but have been optimized more recently to work as wide-band, photon-number resolving detectors to absorb >95% of incident photons at near infra-red (NIR) wavelengths [2]. This high single photon quantum efficiency was instrumental to an experiment on a loophole-free violation of Bell's inequality [3].

Detection of a single photon by the TES leads to an electric pulse response with a fast (tens of nanoseconds) rising edge, and a decay with a time constant of a few microseconds [4]. Straightforward application of time-tagging techniques, such as threshold crossing or constant fraction discrimination (CFD), work well when the pulses are isolated. However, when multiple pulses overlap, they may be incorrectly identified as a single event. Consequently, the apparent number of photons detected is reduced.

To deal with overlapping pulses, several methods have been developed for particle and high-energy radiation detection [1, 5–8]. In [1], Fowler et al. used differentiation in time to better locate the steep rising edge of individual photodetection events when the signals are overlapped: the number of rising edges corresponds to the number of detected photons. The detection times and photon number were then used to initialise a fit to a multi-photon model. This works well when signal-to-noise ratio is high, which is common for the detection of high-energy photons like γ and X-rays.

For near-infrared (NIR) photons detected with a TES, the signal-to-noise ratio is relatively low (SNR=2.4 [9]),

and timing accuracy is affected by the bandwidth limitations necessary to reject false positives.

In this work, we adopt a different approach. We use a 2-level discriminator together with signal integration to count photons emitted from a NIR continuous wave (CW) source, centered at 810 nm. The discriminator does not trigger for noise fluctuations smaller than the difference between the two levels. We then apply least-squares fitting to the signal to recover the amplitudes and detection times of the underlying photon pulses.

II. ELECTRONICS AND PHOTON DETECTION PULSE

We use Tungsten-based TESs provided by a collaboration with NIST [2]. The devices are kept at a temperature of 80 mK using an adiabatic demagnetization refrigerator (ADR) cryostat (Entropy Cryogenics). The first amplification stage consists of a SQUID Series Array (Magnicon C6), followed by further signal conditioning at room temperature (Magnicon electronics XXF-1 [10]) with an overall amplification bandwidth of $\approx$ 6 MHz. The amplifier output has a RMS noise of 1.8 mV. The low frequency components of the noise result in a slowly varying baseline in every trace. We minimise this by operating the SQUID in a flux-locked loop [10]. We record 10 μs long traces with a sampling rate of 0.5 GS/s on oscilloscope with a vertical resolution of 12 bit.

In the rest of this work we indicate the signal as a function of time as $V(t)$. To characterize the TES response, we use a laser diode (LD) centered at 810 nm as a light source, operated in continuous (CW) mode. We control the average photon number with a variable attenuator, then launch the light into a single mode fiber (type SM28e) that directs it to the sensitive surface of the TES.
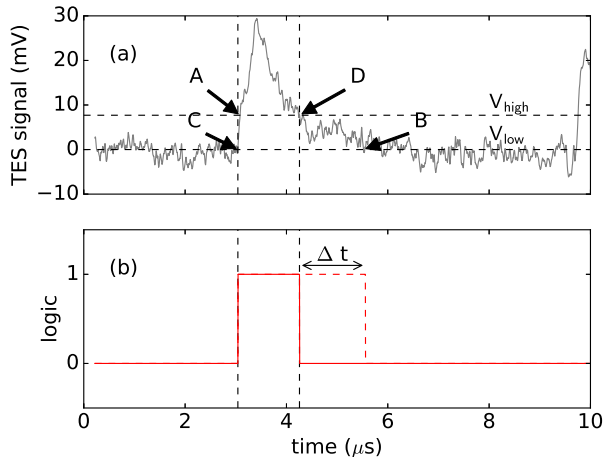
*[*] *jianwei.lee@u.nus.edu

FIG. 1: (a) Two overlapping pulses separated by 233 ns arrive at about 3 μs. The rising edge of the later pulse is obscured by the earlier pulse and prevents detection time estimation using the crossing-time at threshold V_{high}. (b) A two-level discriminator identifies the region CD containing the rising edges of the overlapping pulses. This is the most relevant region of the pulse to consider when identifying the detection times of photons. The region is used to initialise a least-square fit of the signal to a TES response model in order to determine the detection time of the obscured pulse. We extend the region by Δt to include the full pulse when we want to consider its integral. The integral, being proportional to the energy absorbed, is used to count photons. We discard regions that contain partially captured pulses, such as the one appearing on the right edge of the acquisition window.

For light at 810 nm, the signal after the amplifier chain exhibits a rise time for a single photon pulse in the order of 100 ns, and an overall pulse duration of 2 μs. For every recorded pulse trace, we remove the varying baseline,

$$V'(t) = V(t) - V_y \qquad (1)$$

where V_y is the most frequently occurring value of the discretized signal ($V(t)$) over the sampling interval.

III. PULSE IDENTIFICATION

We use the digital equivalent of SET-RESET latch edge detection to detect pulses, with SET triggered when the signal passes threshold V_{high} (Fig. 1 point A) and RESET by the first subsequent crossing of threshold V_{low} (point B).

We determine the threshold V_{high} by considering the distribution of the maximum height of a sample of 4×10^4 traces. The resulting histogram (see Fig. 2), clearly shows two peaks. The lowest voltage peak corresponds to traces without any detection event ($n = 0$), the second one to traces with at least one detection event ($n > 0$). We set V_{high} to the value that minimizes the overlap between the two distributions while V_{low} is set to 0 V.
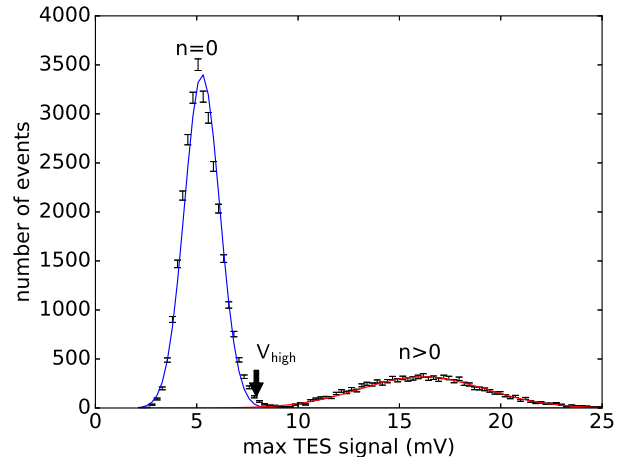

FIG. 2: Maximum TES signal distribution to a continuously running LD with $\bar{n} = 0.25$. The two peaks correspond to 0 and at least 1 photon being detected respectively. Error bars indicate Poissonian standard-deviation. Black arrow: Point of minimal overlap between Gaussian fits to the two height distributions corresponding to $V_{high} = 7.9$ mV.

IV. PHOTON NUMBER DISCRIMINATION

The number of distinct edges identified by the discriminator is not an indication of the number of photodetection events because closely overlapping pulses may be incorrectly identified as a single event.

To determine the number of photodetection events, we assume that the detection and subsequent amplification have a sufficiently linear response, so that the integral of each signal is proportional to the energy absorbed [11].

To increase signal-to-noise ratio, we use the discriminator to identify integration windows surrounding photodetection events (Fig. 1b).

The initially selected region AB identified by the two-level discriminator contains only a fraction of the leading edge belonging to the first pulse. To ensure its inclusion, we consider the first low crossing (point C) before point A as the starting point of the pulse window.

To include the decaying tail, we cannot rely on the crossing of the low threshold (point B), as the signal-to-noise ratio in this region is low. Instead, we extend the integration window by a duration Δt after the last high crossing (point D).

We then compute the pulse area a for every trace, and organize them in histogram $C(a)$. We empirically found a duration $\Delta t = 1300$ ns to optimise the photon-number resolution of $C(a)$.

In this work, we collect traces of finite duration equal to 10 μs, resulting in partial pulses being recorded at the edges of the acquisition window. We reject these events to avoid degradation of pulse-integral distinguishably between signal regions containing complete pulses.
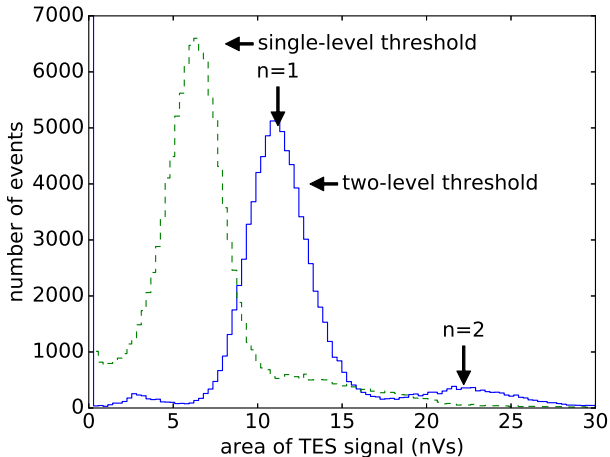
To illustrate the photon number resolving ability of

FIG. 3: Area distribution of 10 μs long traces obtained with different methods: Straightforward integration of the signal above threshold V_{high} (Dashed line) does not yield good photon-number resolution, as it excludes the rising edge and decaying tail of the pulse below threshold. Better resolution is obtained by integrating full pulses identified with a 2-level discriminator while rejecting partial pulses at the edge of the signal traces (Solid line).
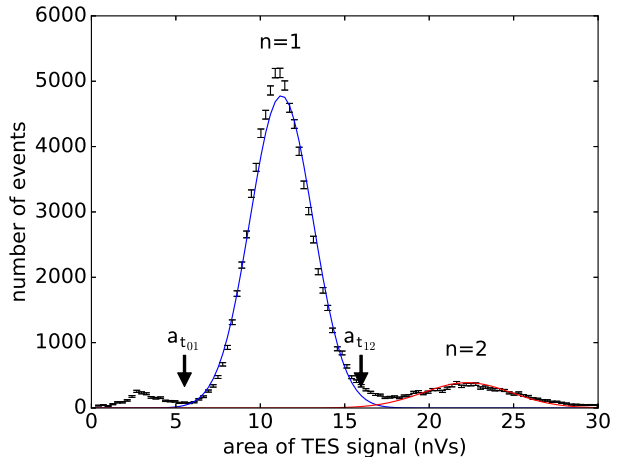

FIG. 4: Pulse area distribution $C(a)$ of the signal in the discriminated region. Events with area below $a_{t_{01}}$ are classified as containing zero photons. Gaussian distributions fitted to the $n = 1$ (Blue) and $n = 2$ (Red) area distributions have a minimal overlap at $a_{t_{12}}$. At this threshold, the probability of falsely attributing the detection of a single photon to a trace containing $n = 2$ photons is 0.6%. Error bars indicate Poissonian standard-deviation.

this method, we compare the area histogram obtained with this method with one obtained from integrating the portion of the trace above V_{high} in Fig. 3. Evidently, the integral distribution obtained using the 2-level discriminator, with partial pulse rejection, has a better resolution power, as events for one or two photons, as well as cases with noise only, can clearly be distinguished from each other.

To obtain clear regions for $n = 0, 1, 2 \ldots$ photons, we fit the distribution $C(a > a_{t_{01}})$ corresponding to $n > 0$ detection events to the sum of Gaussian peaks $G_n(a; a_n, \sigma_n)$:

$$C(a > a_{t_{01}}) = N \sum_{n=1}^{n_{max}} P(n|\bar{n}) \, G_n(a; a_n, \sigma_n), \quad (2)$$

with coefficients P following a Poissonian distribution with average $\bar{n}$ and N the total number of traces.

The Gaussian distributions corresponding to 1 and 2 photons in Fig. 4 demonstrates near linear dependence of the integral with photon energy ($a_2/a_1 = 1.98$).

We determine the minimum overlap between $G_1(a; a_1, \sigma_1)$ and $G_2(a; a_2, \sigma_2)$ to be the threshold $a_{t_{12}}$. At this threshold, the probability of falsely identifying an $n = 1$ trace as an $n = 2$ trace is 0.6%, while the probability of falsely identifying an $n = 2$ trace as an $n = 1$ trace is 0.8%.

V. DETERMINING THE DETECTION TIMES OF OVERLAPPING PULSES

To determine the detection times of overlapping pulses, we rely on least-squares fitting of the signal $V'(t)$ to a multi-photon model $V'_{\text{model}}(t)$ comprising of a linear superposition of N single-photon models $V_{p1}(t - t_n)$:

$$V'_{\text{model}}(t) = \sum_{n}^{N} A_n \, V_{p1}(t - t_n), \quad (3)$$

where N is the number of photons detected within the discriminator window, t_n the detection time, and A_n the maximum pulse amplitude of the n-th photon. We improve the quality of the fit by restricting the time window to the region most relevant to the arrival of the photons (Fig. 1 region CD). An example of the fit result is shown in Fig. 5.

VI. CONCLUSION AND FUTURE WORK

In conclusion, we have successfully resolved between $n = 0, 1$ and 2 photons from a CW NIR source, using the signal integral evaluated in the time window identified by a two-level discriminator.

The time window includes a greater fraction of the TES pulse relevant to photodetection that is usually omitted by a single-threshold discriminator. By considering an optimal fraction of the pulse profile, we obtained pulse integral distributions sufficient to resolve between photon

numbers. This technique provides an alternative to photon counting using edge detection on the differentiated signal, especially when signal-to-noise ratio is low.
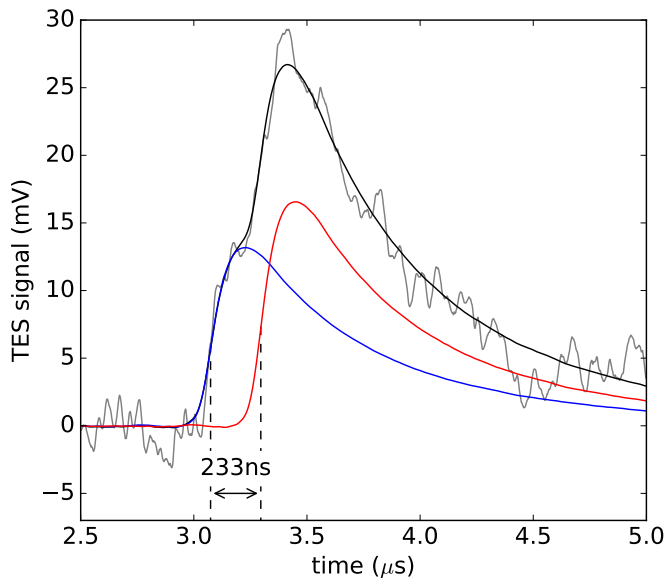

FIG. 5: Fit (black) of a 2-photon signal (grey) composed of individual single photon events (red, blue) separated by 233 ns, comparable to twice the rise time of a single photon pulse. The single photon model was obtained by averaging the TES response to 10^4 single photon events.

We have also demonstrated how the discriminator can be applied to provide a range of values for the detection times of several photons. We can use this range to initialise a least-squares fit of a signal containing several overlapping TES pulses to a multi-photon model, returning the amplitudes and detection times of the individual photons. The fit accuracy of this procedure is currently being characterised.

[1] J. W. Fowler, B. K. Alpert, W. B. Doriese, D. A. Fischer, C. Jaye, Y. I. Joe, G. C. O'Neil, D. S. Swetz, and J. N. Ullom, ApJS **219**, 35 (2015).

[2] A. E. Lita, A. J. Miller, and S. W. Nam, Opt. Express **16**, 3032 (2008).

[3] M. Giustina, M. A. M. Versteegh, S. Wengerowsky, J. Handsteiner, A. Hochrainer, K. Phelan, F. Steinlechner, J. Kofler, J.-A. Larsson, C. Abellán, et al., Phys. Rev. Lett. **115**, 250401 (2015).

[4] A. E. Lita, B. Calkins, L. A. Pellouchoud, A. J. Miller, and S. Nam, *Superconducting transition-edge sensors optimized for high-efficiency photon-number resolving detectors* (2010).

[5] F. Belli, B. Esposito, D. Marocco, M. Riva, Y. Kaschuck, and G. Bonheure, Nuclear Instruments and Methods in Physics Research Section A: Accelerators, Spectrometers, Detectors and Associated Equipment **595**, 512 (2008), ISSN 0168-9002.

[6] G. Tambave, E. Guliyev, M. Kavatsyuk, F. Schreuder, and H. Löhner, IEEE Nuclear Science Symposium Conference Record pp. 2163–2168 (2012).

[7] M. Vencelj, K. Bučar, R. Novak, and H. J. Wörtche, Nuclear Instruments and Methods in Physics Research, Section A: Accelerators, Spectrometers, Detectors and Associated Equipment **607**, 581 (2009).

[8] S. Marrone, E. Berthomieux, F. Becvar, D. Cano-Ott, N. Colonna, C. Domingo-Pardo, F. Gunsing, R. C. Haight, M. Heil, F. Käppeler, et al., Nuclear Instruments and Methods in Physics Research, Section A: Accelerators, Spectrometers, Detectors and Associated Equipment **568**, 904 (2006).

[9] A. Lamas-Linares, B. Calkins, N. A. Tomlin, T. Gerrits, A. E. Lita, J. Beyer, R. P. Mirin, and S. W. Nam, Appl. Phys. Lett. **102**, 231117 (2013).

[10] D. Drung, C. Assmann, J. Beyer, A. Kirste, M. Peters, F. Ruede, and T. Schurig, IEEE Trans. Appl. Supercond. **17**, 699 (2007).

[11] B. Cabrera, R. Clarke, A. Miller, S. W. Nam, R. Romani, T. Saab, and B. Young, Physica B: Condensed Matter **280**, 509 (2000), ISSN 0921-4526.